# Protokoll
Praktikum Quantenphysik

## Geometrical/Topological Phase Measurement in a Neutron Polarimeter

Durchgeführt am 16 Januar, 2015

Protokoll:
1ste Version abgegeben am: 31 August, 2015
Finale Version abgegeben am: 09 Oktober, 2015

Gruppe von:

Danny Milosavljevic (MN: 0826039)
Daryoush Nosraty Alamdary (MN: 1063348)

Verfasst von: Daryoush Nosraty Alamdary

*Universität Wien*
*Fakultät für Physik*

2015
Wien, Österreich

# Contents

**Abstract**

In this experiment we explore the concept of geometrical-phase, which is also known as the Berry-phase, being induced on thermal neutrons in a polarimetric setup. In 1984 M. V. Berry published his influential paper, in which he described the cyclic evolution of the systems under special (adiabatic) conditions, in which an additional phase factor, in addition to the dynamical phase factor, arises. The geometric phase, commonly said, arises from a global change of the quantum system, without any local changes. In general, the measurement of the phase of the system is not a trivial task, and accordingly, in the case of the geometrical phases, it is not possible to detect these phases in a direct measurement. The only way to detect the geometrical phase is using an interferometer. In this experiment we are working with thermal neutrons, which are generated from a TRIGA-reactor, and use a *Ramsey Interferometer*, realized through a spin-measurement in a neutron-polarimeter, to detect these globally induced geometrical phases, interferometrically.

# 1 Introduction

## 1.1 Background and the Aim of the Experiment

Neutrons are massive particles that have no charge (consisting of two up-quarks and two downs-quarks, $\frac{2}{3}e^- + 2(-\frac{1}{3})e^- = 0$), with a mass of $m = 1.675 \times 10^{-27} kg$. A free neutron has a lifetime of $\tau = 889.1 \pm 1.8$, after which it decay into a proton, an electron and an anti-neutrino ($\beta^-$-decay):

$$n \longrightarrow p^+ + e^- + \overline{\upsilon}_e + 0.78 \ \ \text{MeV} \tag{1}$$

Neutrons have a spin of $\frac{1}{2}$ with the magnetic dipole moment of $-1.913\mu N_{us}$, where $\mu N_{us}$ is the nuclear magnetic moment, and they are classified according to the strength of their kinetic energy, in the following way: $\leq 10^{-5}$eV =ultra-cold, $10^{-5} - 10^{-3}$eV=cold, $10^{-3} - 0,5$eV=thermal, $\geq 0,5$eV=hot.

Due to their neutral-charge, the weakness of their interaction, and the depth of their penetration, neutrons are very suitable for radiography, since they pass through condensed matter even with low energies, and therefore they provide a good tool for non-destructive material investigation. Also, due to the fact that the neutrons posses a magnetic dipole-moment, have a mass, and are in the nucleus, they are subject to all four fundamental forces.

In this experiment, we use thermal neutrons in order to measure their geometrical/topological phase, using an experimental setup called a *neutron polarimeter*. Geometrical phase, also know as the *Berry-phase*, is a phase-shift acquired due to the geometrical properties of the parameter space of the Hamiltonian, when the system is subject to the cyclic adiabatic processes. It is the nature of this geometrical phase, that it cannot be measured directly, and therefore using the neutron-polarimeter, we will measure these phases interferometrically. In doing so, we will explore the theoretical predictions that are relevant for this type of phase measurements, such as the behaviour of the geometrical phase with respect to the single, parallel, or opposite rotations of the DC-coils, which induce the geometrical phase. We will also study the effect of different factors, on the quality of our measurements, and the effectiveness of the induction of the geometrical phases through the rotation of the DC-coils. These effects include the orientation and the spatial-adjustment of the DC-coils, and the flipping ratio of these coils, the period of the oscillation of the measurements, and the distance of the path of the neutron beam from the rotation axis of the DC-coils.

# 2 Theory

## 2.1 Larmor Precession of Neutrons in a Magnetic Field

For a free propagating Neutron which is interacting with a magnetic field $\overrightarrow{B}(\overrightarrow{r}, t)$, which excerpts a Torque of $\Gamma = \overrightarrow{\mu} \times \overrightarrow{B} = \gamma \overrightarrow{J} \times \overrightarrow{B}$, the non-relativistic Schrödinger equation is defined by the so-called *Pauli-Equation*:

$$\widehat{H}\Psi(\overrightarrow{r}, t) = \left( -\frac{\hbar}{2m} \overrightarrow{\nabla}^2 - \mu \overrightarrow{\sigma}\, \overrightarrow{B}(\overrightarrow{r}, t) \right) \Psi(\overrightarrow{r}, t) = i\hbar \frac{\partial}{\partial t} \Psi(\overrightarrow{r}, t) \tag{2}$$

with $m$ and $\mu$ being the mass and the magnetic dipole-moment of the neutron, and the $\overrightarrow{\sigma}$, the *Pauli*-operators. The solution to this equation is the following wave-function, in the form of

$$\Psi(\overrightarrow{r},t) = \begin{pmatrix} \Psi_+(\overrightarrow{r},t) \\ \Psi_-(\overrightarrow{r},t) \end{pmatrix} = \phi(\overrightarrow{r},t)|S\rangle \tag{3}$$

where $\phi(\overrightarrow{r},t)$ is the spatial component and the $|S\rangle$, the spin-component of the wave-function.

$$|S\rangle = \cos\frac{\theta}{2}|\Uparrow\rangle + \mathrm{e}^{i\varphi}\sin\frac{\theta}{2}|\Downarrow\rangle \tag{4}$$

The illustration of the $|S\rangle$ which normally only represents a two-level quantum system, could be realized using the *Bloch Sphere*. Furthermore in the presence of an static magnetic field, the polarization-vector of the neutron, $P = \langle S|\overrightarrow{\sigma}|S\rangle$, starts to rotate, for which the equation of motion is given by the following expression, the *Bloch equation*, as it could be seen in the next figure:

$$\frac{d\overrightarrow{P}}{dt} = \overrightarrow{P} \times \gamma\overrightarrow{B} \tag{5}$$

where $\gamma = 2\mu/\hbar$ is the gyromagnetic ratio, and the polarization-vector shows a precession around the external magnetic field $\overrightarrow{B}$ with the Larmor-frequency $\omega_L = |2\mu B/\hbar|$. Figure-[1] illustrates these ideas in geometrical way:

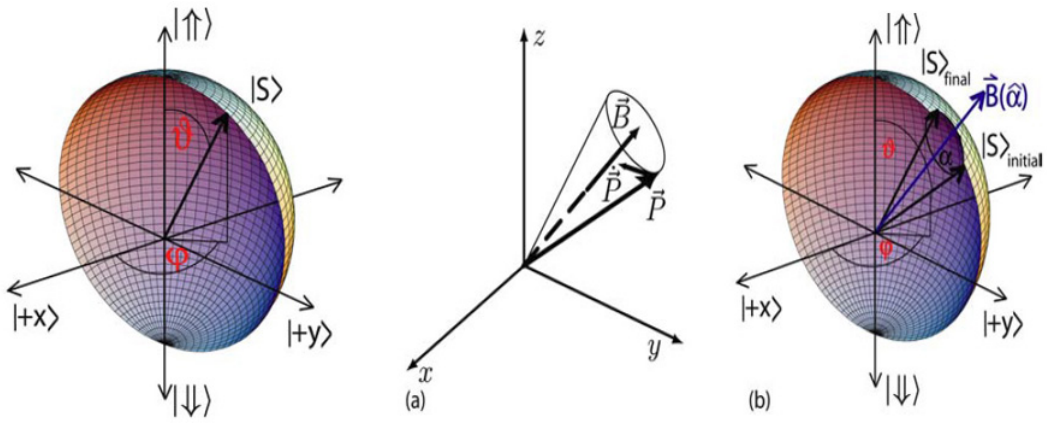


Figure 1: Left: The Bloch-sphere for the illustration of the polarization-vector of the Neutron. Right (center): The rotation of the polarization-vector $\overrightarrow{B}$ under the influence of an external static magnetic field $\overrightarrow{P}$.[1]

The Larmor-precession angle, $\omega_L\tau$, depends solely on two factors: 1- The strength of the applied magnetic field $\overrightarrow{B}$, since the Larmor frequency $\omega_L = -\gamma B$ (with $\gamma$ as the gyromagnetic ratio). 2- The propagation time through the magnetic field $\tau$. One way to realize such a rotation is by DC spin-rotators: a set of coils wrapped around a frame, which induces a 2D static magnetic field in x-, and z-direction. A combination of two of these spin-rotators with an applied phase-shift, with the

[1]Source: Assistance Prof. Yuji Hasegawa, Dr.Stephan Sponar *Quantenpraktikum: Topological Phase Effect in Neutron Optics*, Sommersemester 2014, TU Wien.

spin-rotators acting as $\pi/2$-pulse, is referred to in atomic physics as *Ramsey Interferometer*, which is realized as a polarimeter in Neutron optics. When the spin component of the state-vector of the Neutron goes through the first $\pi/2$-rotator, a superposition-state is created from the initial state $|\Psi_i\rangle = |\Uparrow\rangle$.

$$|\Psi_i\rangle \xrightarrow{\pi/2} |\Psi'\rangle = 1/\sqrt{2}(|\Uparrow\rangle + |\Downarrow\rangle) \tag{6}$$

Before the neutron goes through the second $\pi/2$ rotator, a phase shift $\phi$ is applied using the change of position of the second $\pi/2$-rotator (DC4) along the y-axis. Therefore we have a final state of:

$$|\Psi'\rangle \xrightarrow{\pi/2} |\Psi"\rangle = 1/\sqrt{2}(\mathrm{e}^{-i\phi/2}|\Uparrow\rangle + \mathrm{e}^{i\phi/2}|\Downarrow\rangle) \equiv \frac{1}{\sqrt{2}}(|\Uparrow\rangle + \mathrm{e}^{i\phi}|\Downarrow\rangle) \tag{7}$$

With this superposition state, the probability of measurement of the final state in each of the states $|\Uparrow\rangle$ or $|\Downarrow\rangle$, is given by the expression: $P_{\Uparrow,\Downarrow} = 1/2(1 \pm \cos(\phi))$. This polarimetric technique, which is called *Ramsey Interfermetry* in the case of atomic systems, has the advantage of insensitivity to environmental, mechanical or thermal disturbances, in comparison to *Mach-Zehnder Interferometer*, resulting in higher phase stability.

## 2.2 Berry/Geometrical Phase

The discovery and the understanding of the phase accumulation due to geometrical orientation of the state-vector, is mostly due to the work published by M. V. Berry in 1984, which considered the cyclic evolution of the systems under adiabatic conditions. The significance of this work lies in the fact that it showed the gauge invariance of this phase, which could not be neglected. With that, Berry published in his work that there was an additional phase other than the dynamical one: the geometrical phase.

In order to derive a relatively general argument for the Berry-phase, from which we can apply the expression to our system, we need to consider a quantum system which depends on a multidimensional parameter $R$ parametrizing the Hamiltonian of the system. Therefore the time evolution of the system is defined by the following Schrödinger equation:

$$H[R(t)]|\psi(t)\rangle = i\hbar\frac{\partial}{\partial t}|\psi(t)\rangle \tag{8}$$

The choice of basis for the solution of the equation remains arbitrary, therefore we choose a basis such that the eigenstates are also function of the environments-parameter $R(t)$. With that the eigenvalue problem take the following form:

$$H[R(t)]|n(R(t)\rangle = E_n[R(t)]|n(R(t))\rangle \tag{9}$$

we suppose that the spectrum of the Hamiltonian is discrete and also that the environment and $R(t)$ are varied adiabatically: Adiabatical variation is much slower than the time scale of system during which the system evolves. If the system start in the n-th eigenstate: $|\psi(0)\rangle = |n(R(0))\rangle$. Therefore, according to the adiabatic theorem the system remains in the n-th eigenstate, with the exception of a phase-shift ($\phi$). However the adiabatic theorem does not limit this phase-shift to the

dynamical phase, which is accumulated due to the evolution of the system according to its Hamiltonian:

$$|\psi(t)\rangle = \mathrm{e}^{i\phi_n}|n(R(t))\rangle, \qquad \phi_n(t) = \theta_n(t) + \gamma_n(t) \tag{10}$$

where $\phi$ is the total phase-shift, $\theta_n(t) = -1/\hbar \int_0^t H(t')\mathrm{d}t' = -1/\hbar \int_0^t E_n(t')\mathrm{d}t'$ the dynamical phase, and $\gamma_n(t)$, the Berry (geometrical)-phase. If we insert the equations in (10) into the Schrödinger equation we can determine this additional phase ($R = R(t)$):

$$\begin{aligned} &\frac{\partial}{\partial t}|n(R)\rangle + i\frac{d}{dt}\gamma_n(t)|n(R)\rangle = 0 \\ &\frac{d}{dt}\gamma_n(t) = i\langle n(R)|\frac{\partial}{\partial t}|n(R)\rangle \\ &\frac{d}{dt}\gamma_n(t) = i\langle n(R)|\nabla_R|n(R)\rangle\frac{dR}{dt} \end{aligned} \tag{11}$$

which results in:

$$\gamma_n(t) = i\int_{R_i}^{R_f}\langle n(R)|\nabla_R|n(R)\rangle dR \tag{12}$$

for a cyclic evolution around a closed path $C$ in a time-frame of $T$ such that $R(0) = R(T)$ the Berry phase then is given by the following integral:

$$\gamma_n(C) = i\oint_C \langle n(R)|\nabla_R|n(R)\rangle dR \tag{13}$$

Some of the characteristics of the Berry-phase however, are important to note. In his original paper [4], Berry mentions that "this circuit-dependent" phase-factor can be observed interferometrically , if "the cycled sub-system is recombined with another system, which was separated from it at an earlier time, whose Hamiltonian was kept constant". Therefore this recombination is a requirement for the observation of this phase-factor, in addition to the cyclic evolution of the sub-system under observation. In general however, the Berry-phase is an example of the mathematical notion, which is called *Holonomy*. The holonomy of a connection in differential geometry, on a smooth manifold, is a measure of the extent to which a parallel transport around a closed loop fails to preserve the geometrical data being transported. It is therefore a geometrical consequence of the curvature of the connection. The most common forms of holonomy, which are for connections possessing some kind of symmetry, are each identified with a *Lie group* i.e. the holonomy-group. In the case of Berry-phase, due to broad and unifying implications of the *gauge symmetry*, the topological and geometrical approach to identifying this phase-factor is therefore the more effective approach, compared to trying to solve the equations of motion using the Schrödinger equation.

## 2.3 Example of Spin-$\frac{1}{2}$ particle and Polarimetric Measurement

Consider a spin-$\frac{1}{2}$ particle that moves in an adiabatically rotating magnetic field given by the:

$$\overrightarrow{B}(t) = B_0 \begin{pmatrix} \sin\theta\cos(\omega t) \\ \sin\theta\sin(\omega t) \\ \cos\theta \end{pmatrix} \tag{14}$$

The Hamiltonian and the eigenvalue of this system is given by the following equation:

$$H(t) = \mu \overrightarrow{B} \cdot \overrightarrow{\sigma}, \quad H(t) = \mu B_0 \begin{pmatrix} \cos\theta & e^{-i\omega t}\sin\theta \\ e^{i\omega t}\sin\theta & -\cos\theta \end{pmatrix} \tag{15}$$

$$\Rightarrow H(t)|n(t)\rangle = E_n|n(t)\rangle \Rightarrow E_\pm = \pm\mu B_0, \quad \mu = \frac{1}{2}\frac{e}{m}\hbar \tag{16}$$

$$|n_+(t)\rangle = \begin{pmatrix} \cos\frac{\theta}{2} \\ e^{i\omega t}\sin\frac{\theta}{2} \end{pmatrix} \quad , \quad |n_-(t)\rangle = \begin{pmatrix} -\sin\frac{\theta}{2} \\ e^{i\omega t}\cos\frac{\theta}{2} \end{pmatrix} \tag{17}$$

These eigenstates could be set as spin-up $|n_+(t)\rangle = |\Downarrow_{\overrightarrow{B}(t)}\rangle$ and spin-down $|n_-(t)\rangle = |\Uparrow_{\overrightarrow{B}(t)}\rangle$ with respect to the $\overrightarrow{B}(t)$-direction. In figure-[2], the ideas of the calculation of the solid-angle $\Omega$ in two different situations, movement over the geodesics and the equator, and the movement due to a static magnetic field, along with the polar angle $\theta$ and $\phi$ are illustrated (the angle $\phi = \omega t$):

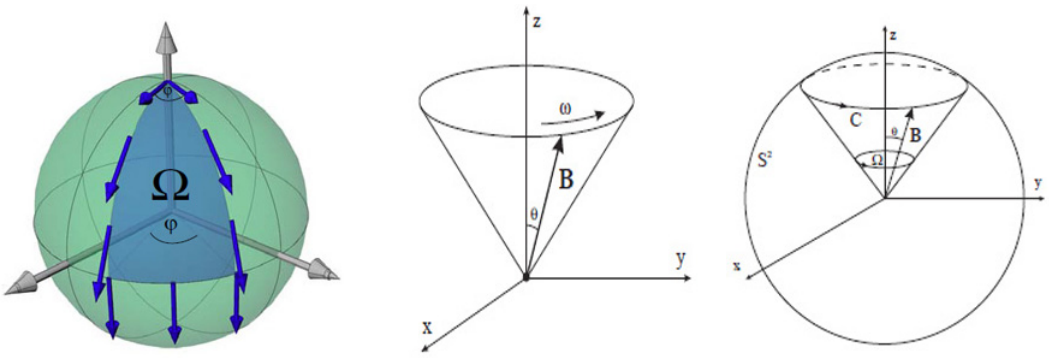


Figure 2: Left: The surface angle $\Omega$ due to movement of spin-vector along the geodesic and the equator. Right (center): The rotation of the spin-vector of spin-$\frac{1}{2}$ particle in the presence of an adiabatically rotating magnetic field $\overrightarrow{B}(t)$.[2]

Now we need to calculate the gradient with respect to the parameter-space, which is spanned by the magnetic field $B(t)$. Therefore we use the gradient in the polar coordinates:

$$\nabla|n_\pm(t)\rangle = \frac{\partial}{\partial r}|n_\pm(t)\rangle\widehat{r} + \frac{1}{r}\frac{\partial}{\partial\theta}|n_\pm(t)\rangle\widehat{\theta} + \frac{1}{r\sin\theta}\frac{\partial}{\partial\phi}|n_\pm(t)\rangle\widehat{\phi} \tag{18}$$

which results in the following expressions:

$$\begin{aligned} \nabla|n_+(t)\rangle &= \frac{1}{r}\begin{pmatrix} -\frac{1}{2}\sin\frac{\theta}{2} \\ \frac{1}{2}e^{i\omega t}\cos\frac{\theta}{2} \end{pmatrix}\widehat{\theta} + \frac{1}{r\sin\theta}\begin{pmatrix} 0 \\ ie^{i\omega t}\sin\frac{\theta}{2} \end{pmatrix}\widehat{\phi} \\ \nabla|n_-(t)\rangle &= \frac{1}{r}\begin{pmatrix} -\frac{1}{2}\cos\frac{\theta}{2} \\ -\frac{1}{2}e^{i\omega t}\sin\frac{\theta}{2} \end{pmatrix}\widehat{\theta} + \frac{1}{r\sin\theta}\begin{pmatrix} 0 \\ ie^{i\omega t}\cos\frac{\theta}{2} \end{pmatrix}\widehat{\phi} \end{aligned} \tag{19}$$

[2]Sources (Figures): Left: Assistance Prof. Yuji Hasegawa, Dr.Stephan Sponar *Quantenpraktikum: Topological Phase Effect in Neutron Optics*, Sommersemester 2014, TU Wien.
Right (and Center): Katharina Durstberger: *Geometric Phases Quantum Theory-Diplomarbeit*, Januar 2002, Universität Wien.

If we then take the scalar product $\langle n|$:

$$\langle n_+|\nabla|n_+\rangle = i\frac{\sin^2\left(\frac{\theta}{2}\right)}{r\sin\theta}\widehat{\phi} \quad , \quad \langle n_-|\nabla|n_-\rangle = i\frac{\cos^2\left(\frac{\theta}{2}\right)}{r\sin\theta}\widehat{\phi} \tag{20}$$

The integration of the above expectation values over the closed curve $C$, while $r = const.\ \ \theta = const.\ \ \phi \in [0, 2\pi]$ yields:

$$\oint_C \langle n_\pm|\nabla|n_\pm\rangle r\sin\theta d\phi\widehat{\phi} = i\pi(1 \mp \cos\theta) \tag{21}$$

Therefore the Berry phase of the equation (12) has the following form for the spin-$\frac{1}{2}$ particle in an adiabatically moving external magnetic field:

$$\gamma_\pm = -\pi(1 \mp \cos\theta) \tag{22}$$

which in terms if the solid angle $\Omega = \int_0^{2\pi}(1 - \cos\theta(\phi))d\phi$ would simply be written as.

$$\gamma_\pm(C) = \mp\frac{1}{2}\Omega(C) \tag{23}$$

In the case of neutrons in our experiment, however the Berry phase is generated using spin-flippers, i.e. DC coils which induce a magnetic field in specific direction which rotate the polarization-vectors 180° about the $y$-axis. If we were to characterize these spin-rotators, using the operator-formalism, they would simply be elements of $SU(2)$-group:

$$U(\beta) = \exp\left(-i\frac{\overrightarrow{\sigma}\,\overrightarrow{\beta}}{2}\right) = \mathbb{1}cos\left(\frac{\beta}{2}\right) - i\overrightarrow{\sigma}\widehat{\beta}\sin\left(\frac{\beta}{2}\right) \tag{24}$$

with $\overrightarrow{\sigma}$ the as the Pauli-operators, $\beta$ the angle from the Larmor precession, and $\widehat{\beta}$ the axis of rotation. Therefore if the initial-state $|\Uparrow\rangle_z$ after the first spin flip $\beta_1 = \pi$ and the second spin flip $\beta_2$, we have the following final state:

$$|\psi_{final}\rangle = U(\beta_2)\cdot|\psi'\rangle = U(\beta_2)\cdot(-i\cos\beta_1 + \sin\beta_1)|\Downarrow\rangle_z = -\mathrm{e}^{i(\beta_1-\beta_2)}|\Uparrow\rangle_z \tag{25}$$

$$= \mathrm{e}^{i(\beta_1-\beta_2+\pi)}|\Uparrow\rangle_z = \mathrm{e}^{i\gamma}|\Uparrow\rangle_z$$

Therefore the geometric (Berry) phase $\gamma = \beta_1 - \beta_2 + \pi$. As mentioned before however, this phase cannot be measured using a direct measurement technique(i.e. the expectation value of an observable), as the expectation value of the Pauli-spin matrices result in:

$$\langle\Uparrow|_z\overrightarrow{\sigma}|\Uparrow\rangle_z = \langle\Uparrow|_z(-\mathrm{e}^{i\gamma})\overrightarrow{\sigma}(-\mathrm{e}^{-i\gamma})|\Uparrow\rangle_z = (0,0,1)^T \tag{26}$$

that is why in order to measure this phase an interferometric/polarimetric setup is required. Since our setup in this experiment is of the polarimetric type, one needs to also keep in mind that the our reference state $|\Uparrow\rangle_z$ also accumulates a geometric phase after the first $\pi/2$-rotation. Therefore the total geometric (Berry) phase measured in the polarimetric setup of our experiment amounts to:

$$\gamma = \gamma_\uparrow - \gamma_\downarrow = 2(\beta_1 - \beta_2) \tag{27}$$

# 3 Experiment

## 3.1 Experimental Setup

### 3.1.1 Neutron Source and the Monochromator

The neutrons used in this experiments, which are generated in a $^{235}$U Fission within the TRIGA-reactor, are thermal neutrons with $25meV$-energy, as they are in an equilibrium with the moderator material (i.e. water). The neutron-beam, are exit through the tangential beam tube which has a lower Gamma-radiation compared to the direct beam tube. The monochromator installed at this beam tube, reflects the neutrons with 3 different wavelengths, 1.7Å, 2Å, 2.7Å. using mosaic crystal made of pyrolytic graphite. The setup is installed on the 1.7Å beam-line with the *Bragg angle* of 28.5°. The figure-[3] illustrates the configuration of the monochromator on the tangential beam tube of the reactor, from which the beams of different wavelengths scatter with different angles:

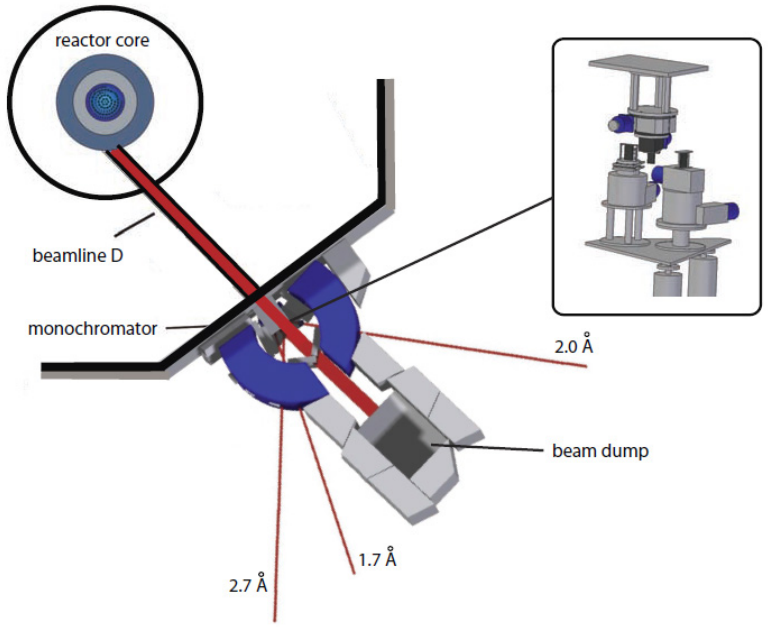


Figure 3: the details of the monochromator setup at the tangential beam tube of the reactor, and the resulting neutron beams of different wavelengths.[3]

### 3.1.2 The Polarimenter and its Components

The setup consists of two filtering devices, the polarizer, and the analyzer, one at upstream and the other one at down-stream, which act as spin-filters. These devices are made up of different layers of different coherent scattering length. There is transmission and also the reflection in percentage of the entire incident beam. The use of alternating magnetic and non-magnetic medium, would require taking into consideration, not only the nuclear scattering length, but also the magnetic scattering length. This can consequently be used for polarization of the beam. The rule for the transmission is that if the sum of the nuclear scattering length and the

[3]Sources: Assistance Prof. Yuji Hasegawa, Dr.Stephan Sponar *Quantenpraktikum: Topological Phase Effect in Neutron Optics*, Sommersemester 2014, TU Wien.

magnetic length of one spin component (i.e. $|\Downarrow\rangle_z$) equal the scattering length of the non-magnetic substance, then this spin component will be transmitted. This construction, which uses a magnetic field, and is used either as polarizer or the analyzer, is known as the *supermirror*.

Between the two devices (the polarizer and the analyzer) at the beginning and the end of the experimental setup, a uniform magnetic field is applied, which is pointing in the $|Z_+\rangle$-direction, and also four DC-coils as spin-rotators, DC1-DC4. The polarized neutrons, which are in $|\Uparrow\rangle_z$-eigenstate, are guided through the setup, throughout which they remain under the influence of the guide field $B_0$, and go through each four of these DC-coils. The first and the last DC-coils, DC1 and DC4 are $\pi/2$-rotators, which create a superposition state $\frac{1}{\sqrt{2}}(|\Uparrow\rangle_z + |\Downarrow\rangle_z)$ out of the initial state $|\Uparrow\rangle_z$, and vice versa. The DC-coils in between, DC2, and DC3 ,are rotators that induce a spin flip ($\pi$-rotator) about an axis in the xy-plane, which make the angles $\widehat{\beta_1}$ and $\widehat{\beta_2}$ with the y-axis. These are the angles from which the geometric phase originates, however the rotation-angles carried out by these DC-coils are $\pi$-rotations. All four DC-coils are adjustable through rotations around $x-$ and the $z-$axes, and the DC4 also slides along the $y$-axis. This configuration enables us to measure the geometric phase induced by the DC2, DC3-coils interferometrically, without which the setup would be an empty polarimeter. The schematic sketch of the setup is illustrated in figure-[4]:

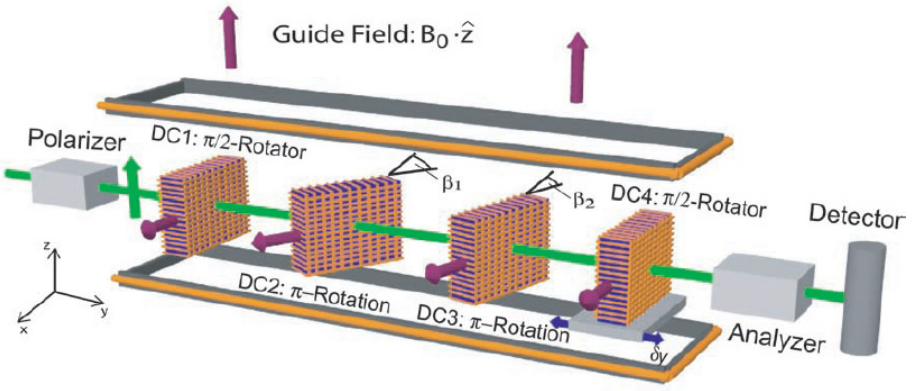


Figure 4: The experimental setup for polarimetric detection of the Berry phase in polarized neutrons flying through uniform magnetic field.[4]

The uniform magnetic guide field, which is applied throughout the experimental setup is in a Helmholtz configuration pointing away from the floor of the setup in the $+z$-direction. The field is applied in order to maintain the polarization of the photons, and is tuned at $\approx 12\ \ Gauss = 1.2\ \ mT$. The magnetic field induced by the DC-coils in $+z$-direction, are applied in conjunction with the guide field in order to compensate the uniform field, where there is non-uniformity. The magnetic field in the $x$-direction, induced by the DC-coils work independent from the guide field and are orthogonal to the direction of the guide field. However, they are adjusted with respect to the strength of the guide field $B_0$, in order to flip the maximum number of neutrons and maintain a prefect Larmor precession throughout the setup. The

[4]Sources: Assistance Prof. Yuji Hasegawa, Dr.Stephan Sponar *Quantenpraktikum: Topological Phase Effect in Neutron Optics*, Sommersemester 2014, TU Wien.

manual control and the scan of the DC-coils using the stepper-motors, plus the reading of the count rates are carried out in *LabView* program in a PC.

## 3.2 Results

### 3.2.1 Adjustment of the Coils

In the first step of the experiment, the the correct flipping current for the DC-coils must be found so that the flipping ratio would correspond to the ideal ratios defined by the rotation angles of the DC-rotators, namely $\pi/2$ and $\pi$. Since DC-2 is supposed to perform a $\pi$-flip, in order to increase the flip-ratio (i.e. the number of $\pi$-flips performed on the incoming neutrons divided by the total number of neutrons), the coil must be parallel to its x-axis. In order to detect and correct any unevenness along the x-axis, the magnetic field along the x-direction, $B_x$, must be varied, to observe the intensity oscillation with the strength of the magnetic field. A perfectly symmetric coil would have an equal minima about the zero-point, which would then perform a perfect $\pi$-flip.

The goal is to adjust the DC2-coil so that the tilt angle $\rho < \pm 1^\circ$ would be achieved. In order to achieve this evenness however, the magnetic field in the $z$-direction induced by the DC-coil must be varied to compensate for the guide field $\overrightarrow{B} = B_0 \cdot \hat{z}$. For the optimization of the flip ratio DC-current along the x-axis was measured at 2.701 A, and the amount of current corresponding to the $\pi$-flip would be chosen, from the minima of the intensity. Afterwards a $B_z$-scan is performed for DC-2 in order to know how much to compensate for the guide field in the $z$-direction. For this purpose also the current corresponding to the minimum count-rate must be selected and set, so that the coil would be even along the x-axis, through the compensation of the $z$-direction magnetic field induced by the DC-coil. Figure-[5] illustrate the first $B_x$-scan and the $B_z$-scan of the DC2-coil:

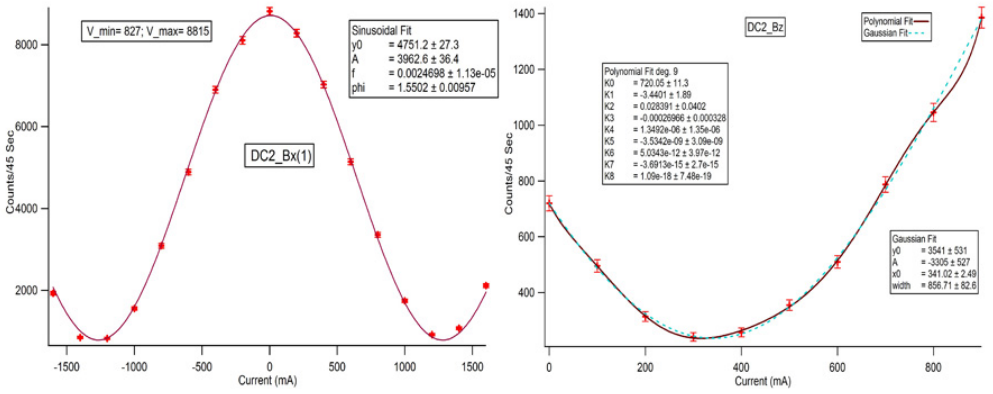


Figure 5: Left: DC2-$B_x$ scan after adjusting the x-axis current for $\rho < \pm 1$ with sinusoidal Fit. Right: DC2-$B_z$ scan after choosing the current for $\pi$-flip from the first $B_x$ scan.

Now despite the adjustment along the x-axis, there is a slight difference between the minima of the $B_x$-scan curve. Therefore we proceed to the $B_z$-scan, which we then fit with a Gaussian and a polynomial fit to determine the current corresponding to the minimum counts. Notice that the polynomial fit is slightly out of shape compared to the Gaussian-fit. Therefore according the Gaussian fit the current for

the minimal $B_z$-counts amounts to $341.02 \pm 2.49$ mA. Following this scan another $B_x$-scan is performed to determine the best value for $\pi$-flip, which is illustrated in the following figure:

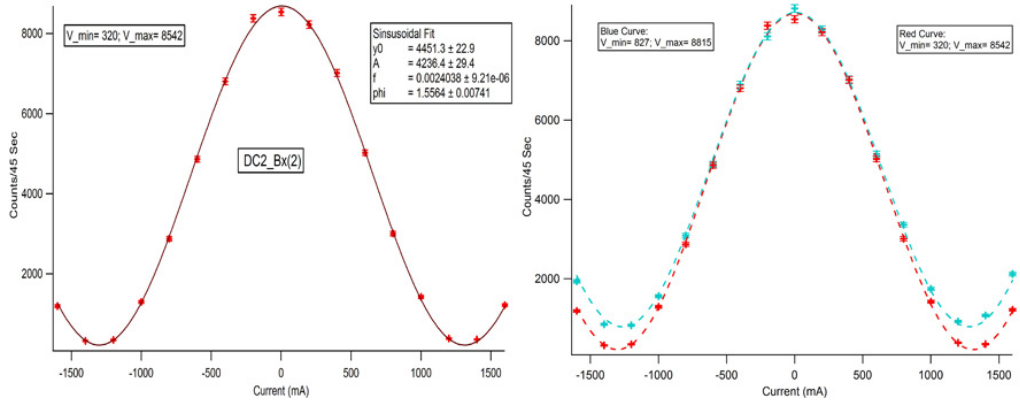


Figure 6: Left: The second DC2-$B_x$ scan after having performed a $B_z$-scan. Right: The comparison of the first and the second DC2-$B_x$-scan.

After the second $B_x$-scan, it is noticeable that the curve is more symmetric, and is evenly distributed range of the current. The other factor that has changed from the first $B_x$-scan is the flipping ratio defined as $R = I_{max}/I_{min}$. According to the statistic of the curves the following flipping ratios have been calculated:

$$R_{B_x(1)} = \frac{8815}{827} = 10.65 \quad , \quad R_{B_x(2)} = \frac{8542}{320} = 26.69 \tag{28}$$

For the $B_x$-current corresponding to the $\pi$-flip of the DC1, and DC4, and $\pi/2$-flip of the DC2 and DC3, which are to be read from the minima of the $B_x$-scan and the $\pi/2$ distance from the minima, the following values are calculated from the sinusoidal fit:

$$I_{(\pi)}(\mathrm{DC1}, 4) = 1312.91 \pm 3.50 \ \ \mathrm{mA} \quad , \quad I_{(\pi/2)}(\mathrm{DC2}, 3) = 659.62 \pm 3.20 \ \ \mathrm{mA} \tag{29}$$

The values of $\pi/2$-flip for DC1, and DC4, and accordingly $\pi$-flip for DC2, and DC3 were set equally, due to the fact that the individual scan for each set of these coils, was not carried out, and the only DC-coil which was scanned for adjustment was DC2. Normally these values differ slightly between DC1-DC4, and DC2-DC3

The above errors were calculated based on the fit-errors using the Gaussian error propagation formula:

$$\Delta I = \sqrt{(\frac{\partial I}{\partial x})^2 \cdot (\Delta x)^2 + (\frac{\partial I}{\partial y})^2 \cdot (\Delta y)^2}$$

### 3.2.2 Measurement of the Geometrical Phase.

For the first measurement, which are performed for single coils rotations ($\beta_1 = 0, \beta_2 = -10, 0, 10$), the DC4 is translated along the $y$-axis, which is the flight-direction for neutrons in order to adjust the count rate which in turn adds an

additional phase shift. The figure-[7] illustrates the intensity oscillations as a result of DC4-translations along the y-axis, without any geometrical phase:

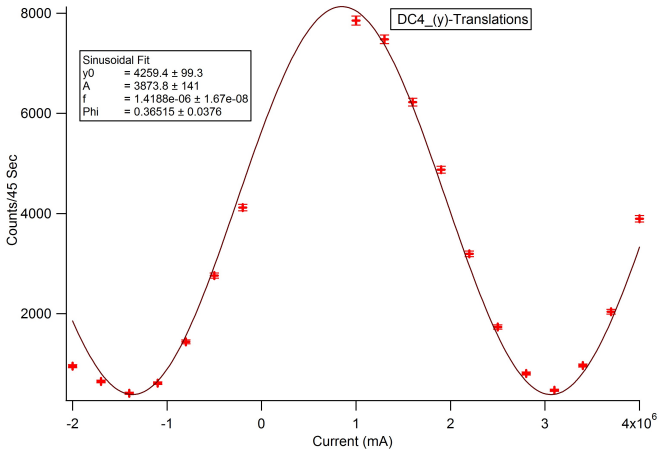


Figure 7: The DC4-(y)-translation intensity oscillation, causing the additional phase shift in addition to the geometrical phase.

The phase shift of the sinusoidal fit in the above curve is $\phi \approx 0.37 \ \ rad = 21.2°$. As it will be seen in the next curves throughout the figures, this amount was indeed added to the geometrical phase that was accumulated, by the neutrons. In figure-[8] the plots of intensity vs. position for the single rotations, i.e. $\beta_1 = 0°, \beta_2 = -10°, 0°, 10°$, are illustrated:

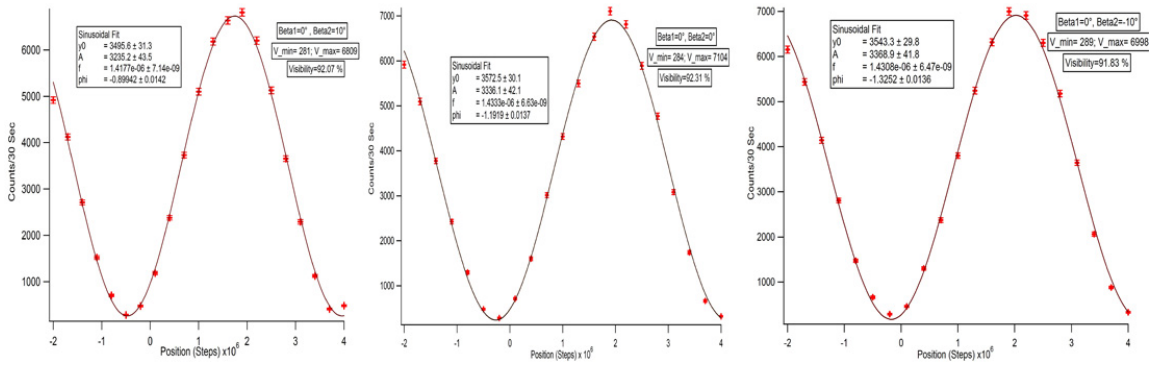


Figure 8: The accumulated geometrical phase shift as a function of the $\beta_2$ angle of DC3, in single coil rotations.

As it could be seen, in the above angle-rotation regime, there is a phase shift as a function of the $\beta_2$, which will be better distinguishable in figure-[9]:

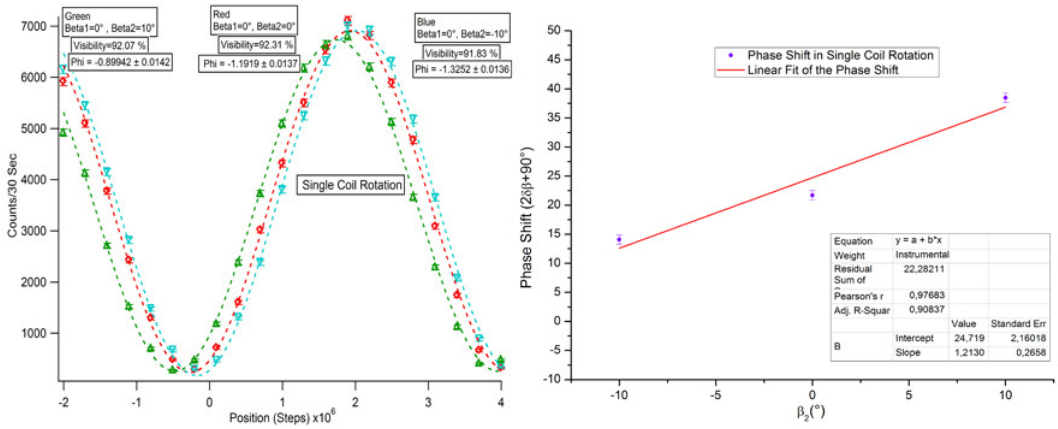


Figure 9: Left: the collective plots of the intensity oscillations in single coil rotations. Right: the linear fit of the geometrical phase shift (+90°) as a function of $\beta_2$.

In the above three intensity plots the curve visibility was also calculated, and average over the 3 curves, and eventually the phase shift was plotted as a function of the $\beta_2$ and fitted linearly:

$$V_{avg} = \left( \sum_{i=1}^{3} \frac{I_i^{max} - I_i^{min}}{I_i^{max} + I_i^{min}} \right) /3 = 92.07\% \quad , \quad \text{Slope}(linear \quad fit) = 1.21 \pm 0.27$$

For a better estimation of the error, which flows into the measurement of the geometrical phase-shift, the period of the oscillations also must be taken into account. The following value is the period of the oscillation for the ($\beta_1 = \beta_2 = 0°$)-configurations:

$$(4.3837 \pm 0.0095) \times 10^6 \quad steps$$

This oscillation period should have been fixed for other configurations as well. However, the period of oscillation varies in two other configuration of the above set in the range of:

$$[(4.4319 \pm 0.0088) - (4.392 \pm 0.0097)] \times 10^6 \quad steps$$

With this range of values, the variations of the period of oscillations contribute to the measurement errors. The exact amount of error however could not be estimated trivially due to the difference of the oscillation-periods, however the amount of error corresponding to this amount difference could bot be negligible.

Similarly the following set of plots illustrate the Intensity oscillation as a function of position of the DC-coils for each of $\beta_2$ in a parallel coil rotations i.e. $\beta_1 = \beta_2 = -10°, 0°, 10°$:

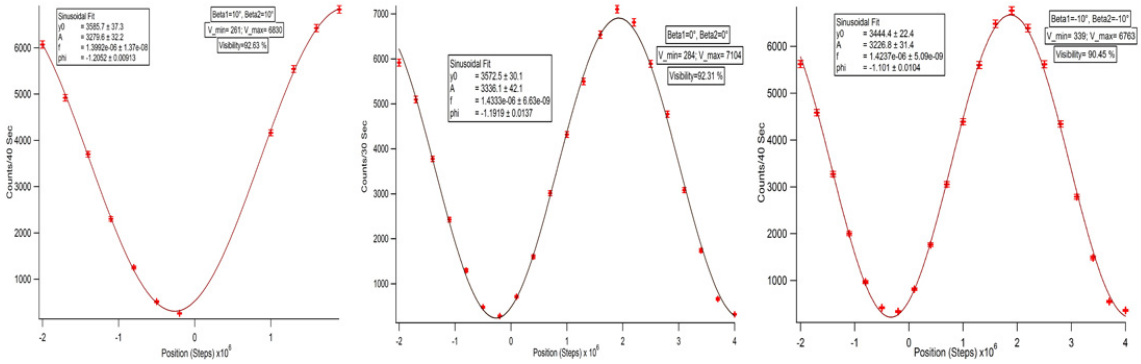


Figure 10: The accumulated geometrical phase shift as a function of the $\beta_2$ angle of DC3, in parallel coil rotations.

contrary to the previous case however, in parallel rotations the phase shift tends to remain unchanged for any change of $\beta_2$. The following plots also illustrate and confirm this fact:

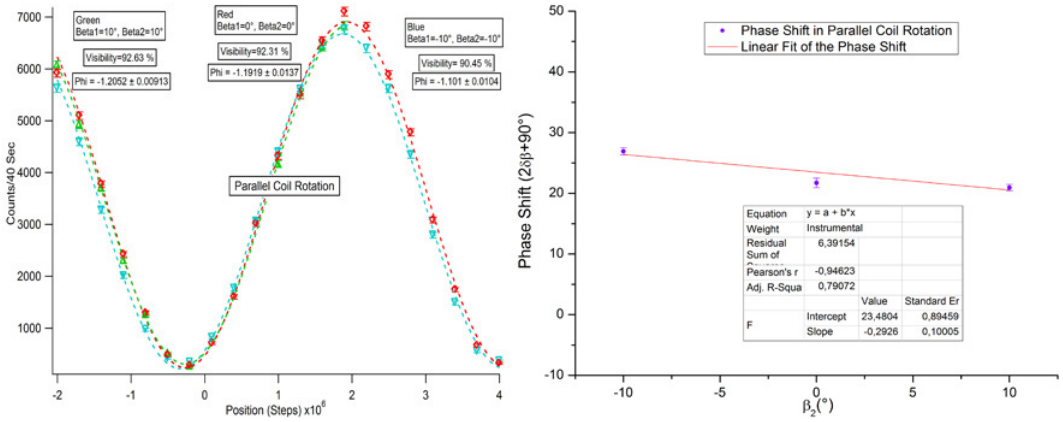


Figure 11: Left: the collective plots of the intensity oscillations in parallel coil rotations. Right: the linear fit of the geometrical phase shift (+90°) as a function of $\beta_2$.

The following are the average visibility of the 3 curves, and the computed slope of the linear fit of the phase shift, plotted as a function of the $\beta_2$:

$$V_{avg} = \left( \sum_{i=1}^{3} \frac{I_i^{max} - I_i^{min}}{I_i^{max} + I_i^{min}} \right) /3 = 91.8\% \quad , \quad \text{Slope}(linear \quad fit) = -0.29 \pm 0.1$$

For the above set of rotations ($[\beta_1 = \beta_2 = 10°]$—$[\beta_1 = \beta_2 = -10°]$), the difference between the period of oscillations ranges from:

$$[(4.4905 \pm 0.0458) - (4.4132 \pm 0.0012)] \times 10^6 \quad steps$$

With this range of variations, in the period of oscillations, the amount of error caused by the variations would be considerable.

And finally the following set of plots were prepared to illustrate the Intensity oscillation as a function of position of the DC4-coil for $\beta_2$ in a opposite coil rotations i.e. $\beta_1 = -\beta_2 = -10°, 0°, 10°$:

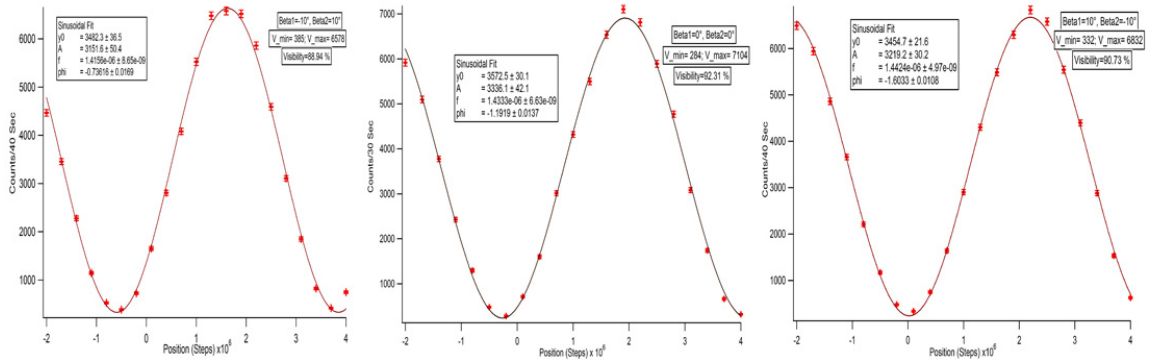


Figure 12: The accumulated geometrical phase shift as a function of the $\beta_2$ angle of DC3, in opposite coil rotations.

In opposite coil rotation similar to the single coil rotation, the accumulated geometrical phase tend to change with the $\beta_2$-angle, however it turns out that the slope of the linear fit i.e. the rate of the change of the phase with the change of the $\beta_2$-angle has increased:

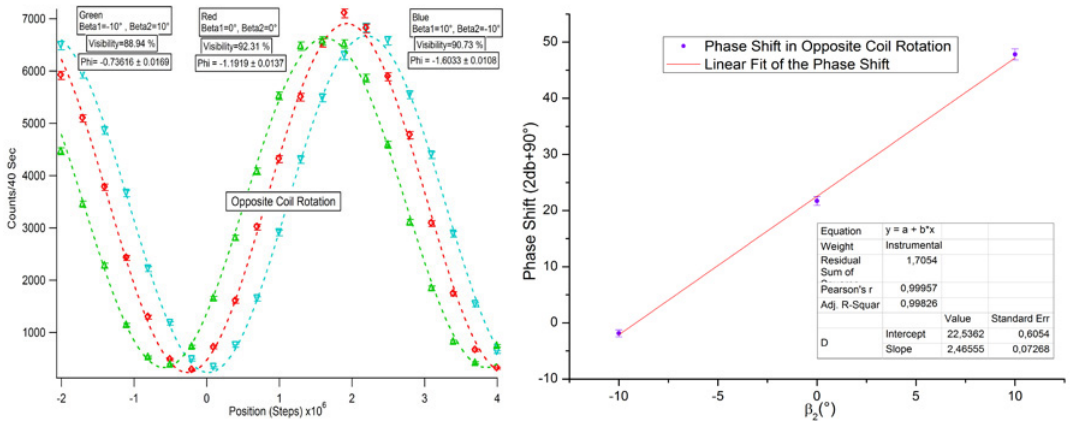


Figure 13: Left: the collective plots of the intensity oscillations in opposite coil rotations. Right: the linear fit of the geometrical phase shift (+90°) as a function of $\beta_2$.

And the following are the average visibility of the 3 curves, and the computed slope of the linear fit of the phase shift, plotted as a function of the $\beta_2$:

$$V_{avg} = \left( \sum_{i=1}^{3} \frac{I_i^{max} - I_i^{min}}{I_i^{max} + I_i^{min}} \right) /3 = 90.66\% \quad , \quad \text{Slope}(linear \quad fit) = 2.466 \pm 0.073$$

Once again an estimation of the difference in the period of oscillations from ($[-\beta_1 = \beta_2 = 10^\circ]$—$[-\beta_1 = \beta_2 = -10^\circ]$) yields:

$$[(4.4385 \pm 0.0007) - (4.3561 \pm 0.0013)] \times 10^6 \quad steps$$

As we can see, in the case of the opposite rotations also, the difference between the oscillation-periods are in a significant range from the value for the central configuration $\beta_1 = \beta_2 = 0^\circ$. This range of difference additionally, similar to the values for single- and parallel rotations, would result in an error in the measurements of the phase-shifts.

# 4 Conclusion & Perspective

In the adjustment part of the experiment, where the coils were to be adjusted for the measurement of the geometrical phase, the processes carried out for DC2 seemingly increased the visibility and the flipping ratio of the coil. The unadjusted coil had a flipping ratio of only $\approx 10$, while after the adjustments the ratio was increased to $\approx 27$. However, in comparison to the sample performed in the experiment's manual, where a perfect phase shift is observed in a single coil rotation, the optimized flipping ratio is $\approx 57$. Therefore, we identify this relatively small flipping ratio as one of the error sources.

Additionally, the variations in the period of oscillations, with respect to the central angle configuration of $\beta_1 = \beta_2 = 0^\circ$, are also a source of error, due to the fact that all the angle settings left of the central configuration have a larger period of oscillation that the central angle-setting $\beta_1 = \beta_2 = 0^\circ$. This in turn reduces the amount of phase-shift as a function of increasing-$\beta 2$. In opposite rotation the right side angle-setting $-\beta_1 = \beta_2 = -10^\circ$, also has a smaller period, which additionally causes a decrease in the phase-shift. Therefore, in total, the shift in the period of oscillations contribute a considerable amount to the error in the measurement of the geometrical phase-shift.

However, aside from the two factors mentioned above, the main source of error in the measurement of the geometrical phase is considered to be the deviation of the neutron beam-path from the axis of the rotations of the DC-coils. For a DC-coil of 5 $cm$-length, the deviation of the beam-path is thought to be $\approx 6$ $mm$ from the rotation-axis of the DC-coil. The applied magnetic field of the coils 15 $Gauss$, together with the neutron velocity of 2 $km/s$, cause the path deviation to effectively reduce the rotation-angles, by a significant amount. In the case of the single rotations, in which the total manual rotation of the $\beta_2$ must be 20°, the beam-path deviation would effectively reduce this angle to $\approx 16$ $degree$. That means that alone the beam deviation has cause the slope of the linear fit in figure-[9] to be reduced to 1.61 from the theoretically correct amount of 2.00. The rest of the reduction in the slope is attributed to the other two error sources mentioned in the above paragraph. Regarding the neutron beam-path deviation, figure-[14] is a graphical illustration of the error estimation due to the distance between the beam-path and the rotation-axis of the DC-coil:

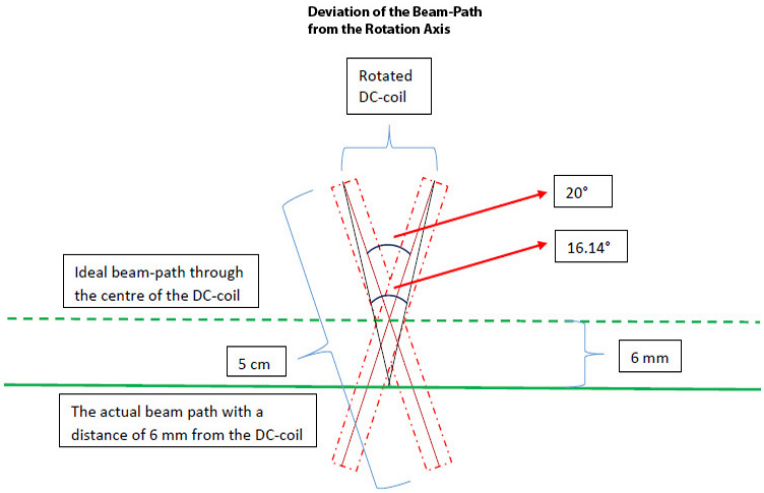


Figure 14: The illustration of the beam-path divergence, from the rotation-axis of the DC-coil, and the estimation-principle of the error in the measurement of the geometrical phase.

Finally with regard to the phase shift as a function of the $\beta_2$, which is angle between DC3 and DC4, all the above regimes demonstrate a agreement with the theoretical predictions. Figure-[15] is once again a collective illustration of the phase shifts:

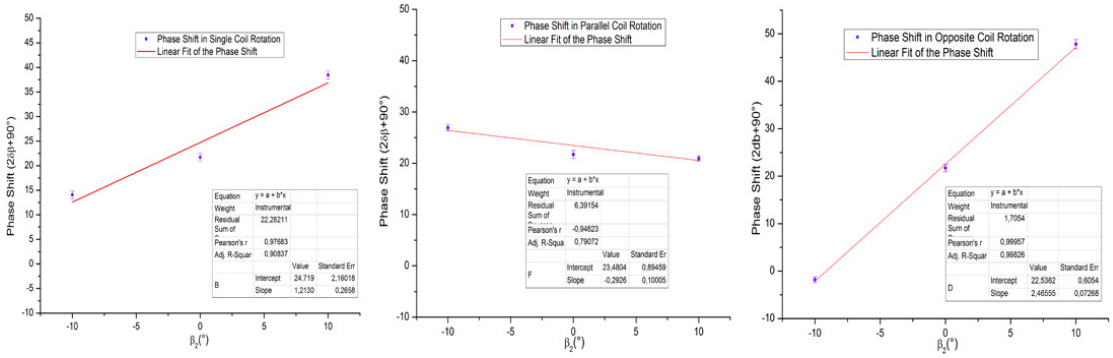


Figure 15: the collective plots of phase shift (+90°) as a function of $\beta_2$ in (from left) *single-* , *parallel-*, and *opposite*-rotations.

According to the theory, in a single rotation regime the total geometrical phase is a function of $\beta_2$ according to the following relation: $\gamma = 2(\beta_1 - \beta_2)$ $\beta_1 = 0° \Longrightarrow \gamma = 2\beta_2$. Therefore the slope of the linear fit in the single coil rotation phase shifts has to be $\approx 2$, which is also the case in the example within the experiment's manual. Here however our measured slope only amounted to $\approx 1.21$ with a margin of error, and the reason for that can only be traced back to the small flipping ratio compared to $\approx 57$. This in turn could be due to the strength of the magnets in DC-coils, which may have varied in time in comparison to the time of the previous measurements included in the experiment's manual

A similar statement could be made for the cases of the opposite and parallel rotations, in which, in one of rotation schemes, parallel rotations, the phase shift

is expected to remain unchanged: $\gamma = 2(\beta_2 - \beta_2) = 0°$. Our measurements in this case show a slight phase shift, where the slope of the linear fit is only $\approx -0.29$. Therefore we conclude one again the agreement of the measurements with the theoretical predictions. Also in the case of the opposite rotations, where the expected phase shift is supposed to change with the rotation angle $\beta_2$, with the ratio of 4: $\gamma = 2(\beta_2 + \beta_2) = 4\beta_2$, the measured slope doubled compared to the single rotations case with $\approx 2.47$. Therefore based on these measurements, taking into account the accumulated error caused by the aforementioned sources, we can conclude that the experimental results agree with the theoretical prediction about the accumulated Berry(geometrical) phase, in a neutron-polarimetric setup, induced by the *probe system* of DC2 and DC3.

# 5 References


[1] Assistance Prof. Yuji Hasegawa, Dr.Stephan Sponar *Quantenpraktikum: Topological Phase Effect in Neutron Optics*, Sommersemester 2014, TU Wien.

[2] Katharina Durstberger: *Diplomarbet: Geometrical Phases in Quantum Theory*, (Jan 2002), Betreut von: Prof. Reinhold A. Bertlmann, 2002 Universität Wien.

[3] *Wikipedia: Geomteric Phase*; https: //en.wikipedia.org/wiki/Geometric_phase, modified on 28 August 2015. Accessed on 10 September 2015.

[4] M. V. Berry, *Quantal phase factors accompanying adiabatic changes*, Proc. R. Soc. Lond. A 392 (1984), 45.

[5] *Wikipedia: Holonomy*; https: //en.wikipedia.org/wiki/Holonomy, modified on 1 September 2015. Accessed on 04 Oktober, 2015.

[6] Josef W. Zwanziger; Mariane König; Alexander Pines *Berry's Phase*, Lawrence Berkeley Laboratory and University of California, Berkeley, California 94720; Annu. Rev. Phys. Chem. 1990. 41:601-46